Intrinsic-extrinsic size effect relationship for micromechanical tests

Janelle P. Wharry [a],*, Kayla H. Yano [b], Priyam V. Patki [b]

[a] School of Nuclear Engineering, Purdue University, 400 Central Drive, West Lafayette, IN 47907, USA
[b] School of Materials Engineering, Purdue University, 701 West Stadium Avenue, West Lafayette, IN 47907, USA

ARTICLE INFO

ABSTRACT

Miniaturized mechanical tests are commonly utilized to evaluate properties of materials, including thin films, nanostructured, and irradiated materials. However, the specimen size effect occurs when miniaturized sample geometries contain too few dislocation sources, resulting in elevated yield stresses. The size effect is controlled by extrinsic (specimen dimensions) and intrinsic (microstructure) factors. Here, we summarize extrinsic and intrinsic size effects from micro-compression pillar, micro-cantilever bend, and flexure studies reported in the archival literature. We find an approximately linear relationship between intrinsic and extrinsic size effects. Meaningful mechanical properties can be measured when extrinsic size dominates the intrinsic size.

© 2018 Acta Materialia Inc. Published by Elsevier Ltd. All rights reserved.

Miniaturized mechanical tests are becoming evermore commonplace for assessing performance of volume-limited materials such as thin films, nanostructured or nanolayered materials, ion irradiated layers, and radioactive or otherwise hazardous specimens. Many of these tests are conducted *in situ* in either a scanning electron microscope (SEM) or transmission electron microscope (TEM), which enable researchers to gain deeper insight into fundamental mechanical behaviors by enabling qualitative observation of plastic phenomena simultaneous to recording of quantitative load-displacement data. However, miniaturized mechanical test specimens have smaller dimensions than prescribed by ASTM standards. Hence, the specimen size effect [1–7] limits the specimen dimensions at which one can accurately and meaningfully obtain both quantitative and qualitative mechanical insights.

The specimen size effect arises when nanoscopic through microscopic mechanical testing geometries are so small that their deformation mechanisms differ from those of bulk specimens. These differing deformation mechanisms often arise because miniature specimens contain too few dislocation sources, so plastic yielding cannot occur until a sufficient population of dislocations has been introduced into the specimen from external loading. Consequentially, the measured yield strength exceeds "bulk" values, and can approach the theoretical strength of the material (blue curve, Fig. 1). When yield strength is controlled by the availability of a dislocation source, *i.e.* **intrinsic** size effect, the yield strength exhibits a negative logarithmic relationship with the specimen dimension. Upon increasing the specimen dimension, one will eventually reach the "transition dimension", at which the yield strength is specimen size-independent. That is, the specimen

dimensions, or **extrinsic** size effects, are sufficiently large that the tested volume contains ample dislocation sources. It has been shown that stochasticity of dislocation source lengths can sufficiently rationalize the onset of the size effect for decreasing specimen sizes [8].

Microstructural refinement, such as through nanostructuring or irradiation, reduces the extent of the specimen size effect by creating a larger number density of obstacles, enabling one to test progressively smaller volumes [9,10]. The overall yield stress is governed by the superposition of dislocations, grain boundaries, and dispersed obstacles of varying morphologies. It is theorized that the higher the number density of dispersed obstacles, the lower the transition dimension [9,10] (red curve, Fig. 1). The transition dimension is inherently correlated with the material microstructure, and understanding this extrinsic-intrinsic size effect relationship is instructive for researchers using miniature mechanical testing methods. The intrinsic size effect is represented as the average obstacle spacing on the glide plane (L_{ob}), which assumes a homogeneous microstructure, from [11]:

$$L_{ob} = \frac{1}{\sqrt{N_{ob}\overline{d_{ob}}}} \tag{1}$$

in which N_{ob} is the total number density of obstacles hindering dislocation slip (*e.g.* loops, stacking fault tetrahedra (SFT), nanoclusters) and $\overline{d_{ob}}$ is the weighted average diameter of the obstacles. If the pillar dimensions are greater than the obstacle spacing, the obstacles are the limiting factor governing dislocation source size [9,12]. Conversely, if there are too few obstacles within a pillar (*i.e.* minimum pillar dimension approaches L_{ob}), the pillar size more significantly influences the dislocation source size, leading to an observed size effect on the measured yield strength.

* Corresponding author at: 400 Central Drive, West Lafayette, IN 47907, USA.
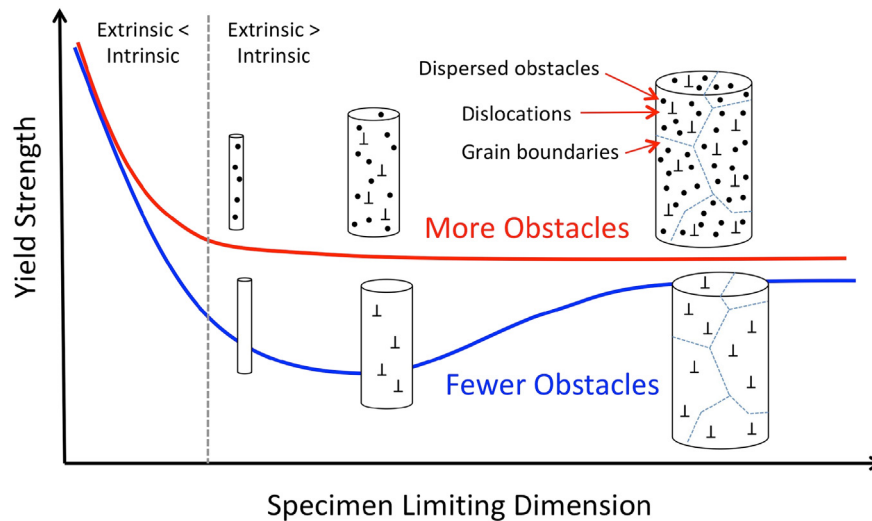E-mail address: jwharry@purdue.edu (J.P. Wharry).

Fig. 1. Illustration of the specimen size effect and the influence of irradiation, with transition dimension indicated by vertical dashed line. (For interpretation of the references to color in this figure, the reader is referred to the web version of this article.)

In this paper, we review the literature to identify an extrinsic-intrinsic size effect relationship for micro-mechanical testing configurations including micro-compression pillars, micro-cantilevers, and thin film flexure. We summarize studies from nine materials; these studies measure yield strength as a function of specimen dimensions and provide sufficient microstructural characterization to estimate the intrinsic size effect (L_{ob}). Although the objectives of the summarized studies were not necessarily to determine a transition dimension, a transition dimension can be estimated from the studies' plots of yield strength *vs.* specimen dimension.

Three of these studies [13,14] utilize TEM *in situ* compression pillars to systematically measure the transition dimension (*i.e.* extrinsic size effect) as a function of microstructure (*i.e.* intrinsic size effect), both before and after irradiation. The first of these studies focuses on an Fe-9% Cr oxide dispersion strengthened (ODS) alloy, which is a candidate for advanced nuclear reactor structural and cladding components [15–20]. The second study focuses on a nanocrystalline Cu-10Ta alloy, which is a model system for more complex engineering ODS alloys, and also exhibits excellent creep resistance [21]. The third study focuses

on pure Cu, and illustrates the influence of irradiation on transition dimension [9]. Results from these aforementioned studies are placed in context of transition dimension results compiled from the archival literature on non-irradiated materials. None of the summarized studies carried out experiments that would enable direct verification that micropillars and bulk specimens deform by identical mechanisms. However, their systematic observations of a transition dimension sufficiently demonstrate that mechanical properties of nano/micro-scopic and bulk specimens can be comparable above that transition dimension. Finally, we determine a relationship between the intrinsic and extrinsic size effect.

Irradiated Fe-9%Cr ODS – Yano et al. [13] studies an Fe-9%Cr ODS martensitic steel irradiated with 5.0 MeV Fe^{2+} ions to doses of 3 displacements per atom (dpa) and 100 dpa at 500 °C. TEM *in situ* compression pillar dimensions are varied 100–600 nm in height and width, and 50–600 nm in thickness. Details of the pillar shaping, testing, and recording processes are provided in ref. [13]. Fe-9%Cr ODS pillars contain oxide nanoclusters and discrete dislocations prior to loading (Fig. 2a). During loading, plasticity occurs in dislocation bursts [13], with the
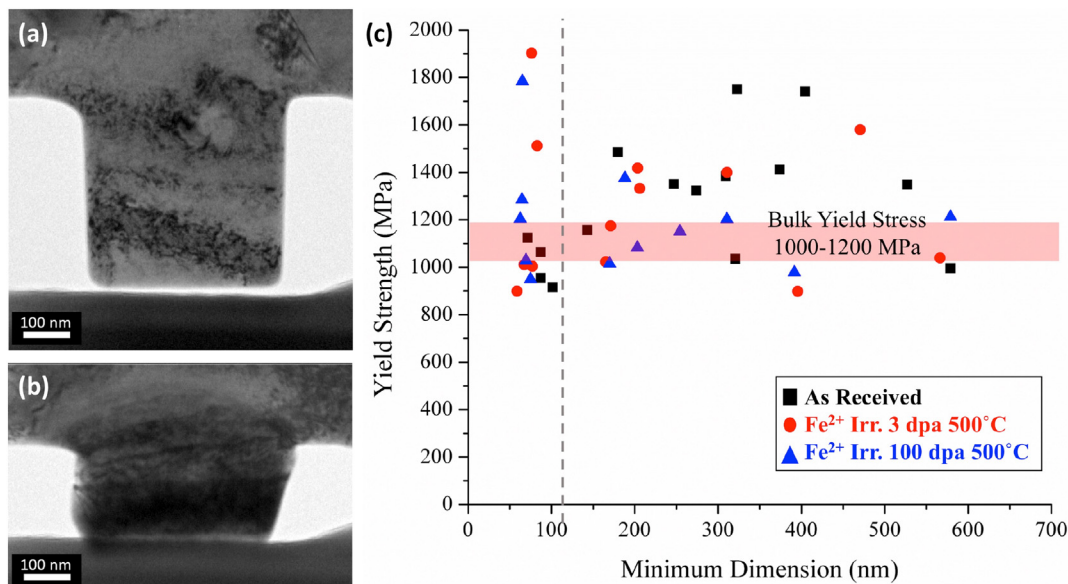

Fig. 2. Representative TEM *in situ* pillar compression still frames from 100 dpa, 500 °C, Fe^{2+} irradiated Fe-9%Cr ODS, showing (a) discrete dislocations before compression testing, and (b) dense dislocation network after compression; (c) yield strength as a function of pillar dimension.

final compressed pillar containing a dense forest of dislocations (Fig. 2b). These TEM video still-frames underscore the role of dislocations in deformation of Fe-9%Cr ODS, suggesting there is a pillar dimension at which the yield strength transitions from pillar size-independent to dislocation source-limited. Yano et al. [13] demonstrates that this transition dimension for Fe-9%Cr ODS is likely to occur within the range 150–200 nm. Specifically, the as-received Fe-9%Cr ODS pillars containing a minimum dimension ≳150 nm have yield strengths that fall within the 95% confidence interval around the bulk yield strength of 1000–1200 MPa [22]. Irradiated Fe-9%Cr ODS pillars do not exhibit a statistically significant change in yield strength [13], consistent with expected values from nanoindentation [23,24]. Increases in yield strength due to the irradiation-induced nucleation of dislocation loops are offset by the softening attributed to partial dissolution of oxide nanoclusters [25–27]. The Fe-9%Cr ODS size effect is illustrated in Fig. 2c, after ref. [13]. Although there is considerable scatter in the data, there may be a transition dimension near 150 nm, above which the yield strength is relatively independent of pillar size.

A combination of TEM and atom probe tomography (APT) are used to quantify the size and number density of grains, phases, dislocation loops, and oxide nanoclusters [25,28,29]. Based on this microstructure characterization [13,25,27], the average obstacle spacing in the Fe-9% Cr ODS ranges 19.9–37.6 nm. Typically, obstacle spacing is determined on the planes on which slip is occurring. However, since the material is nanostructured, even the smallest pillars tested are polycrystalline. As such, multiple slip systems are active in the pillars, so it is not appropriate to measure obstacle spacing only on a single glide plane.

Irradiated Cu-10Ta – Patki [14] studies nanostructured Cu-10Ta (at. %), consolidated from mechanically alloyed powders by equal channel angular extrusion (ECAE) [30]. The CuTa specimens are subsequently irradiated with 2.0 MeV protons to 1 dpa at 500 °C. TEM *in situ* compression pillars are created and tested, having a range of dimensions, following similar methods described by Yano et al. [13]. The Cu-10Ta pillars contain Ta nanophases embedded within a Cu matrix (Fig. 3a). During deformation, the comparatively softer Cu matrix deforms readily, while the harder Ta phases remain relatively undeformed [14], and the final compressed pillar contains contrast from the dislocations that enable the Cu deformation (Fig. 3b). Patki [14] shows that there is no obvious transition dimension for Cu-10Ta. Although the plot of yield strengths against pillar minimum dimension (Fig. 3c, adapted from ref. [14]) exhibits considerable scatter, the measured yield strengths are relatively independent of pillar size, for both the as-received and

irradiated materials. Because of the extensive population of dislocations in the pillars throughout the deformation process, it is not likely that the pillars are already smaller than the transition dimension. Rather, a transition dimension is likely smaller than the smallest pillar tested, *i.e.* ≤100 nm. Overall, the pillars tend to exhibit yield strengths lower than the expected bulk yield strength of 1.23 GPa [30], due to the high strain rate of the TEM *in situ* testing [6,31,32]. The Cu-10Ta exhibits an incremental change in yield strength with irradiation, which is linked to the irradiation stability of the Ta phases as well as the nucleation of irradiation-induced SFTs [14].

The microstructure characterization accounts for Cu grains, Ta nanophases, and irradiation-induced stacking faults. Based on the microstructure characterization [14], the average obstacle spacing in Cu-10Ta ranges 21.2–21.4 nm. Much like the Fe-9%Cr ODS, the nanostructure produces polycrystalline pillars in which multiple slip systems are active. Hence, an overall average obstacle spacing is noted.

Irradiated Cu – Kiener et al. [9] conduct a TEM *in situ* pillar compression study on proton irradiated Cu. They test a range of pillar diameters and measure yield strength as a function of diameter. They observe a distinct transition dimension in the irradiated Cu at ~400 nm (see Fig. 3 in ref. [9]). All defects, including irradiation-induced SFTs and excluding long dislocation lines, are reported to have obstacle spacing on the glide plane, L_{ob} of 68 ± 30 nm.

Ni-base ODS Alloy – Girault et al. [12] utilize *in situ* SEM for their pillar compression studies on Ni-base ODS alloy Inconel MA6000, nominally Ni-15Cr-4.5Al-2.5Ti-2Mo-4W-2Ta-0.15Zr-0.01B-0.05C-1.1Y$_2$O$_3$, in wt.%. They measure a critical resolved shear stress (CRSS) as a function of pillar diameter, and compare their measurements to those from Ni single crystal (see Fig. 3 in ref. [12]). Neither the MA6000 data nor the Ni single crystal data exhibit an inflection point indicative of the transition dimension, unlike the Fe-9%Cr ODS, Cu-10Ta, and Cu data sets [9,13,14]. However, Girault surmises that the MA6000 size effect will be observed when the MA6000 data set intersects with the Ni single crystal data set, at pillar diameters <200 nm. Girault's MA6000 microstructure is characterized in earlier reports, enabling one to estimate an average obstacle spacing of ~50 nm based on their reported populations of oxide dispersoids and dislocation segments. An average obstacle spacing is used here as an estimate to L_{ob} since the microstructural details are reported as a volumetric average rather than on a specific glide plane.

Pure Ni – The aforementioned pure Ni data set to which the MA6000 could be compared, can also provide an estimated transition dimension
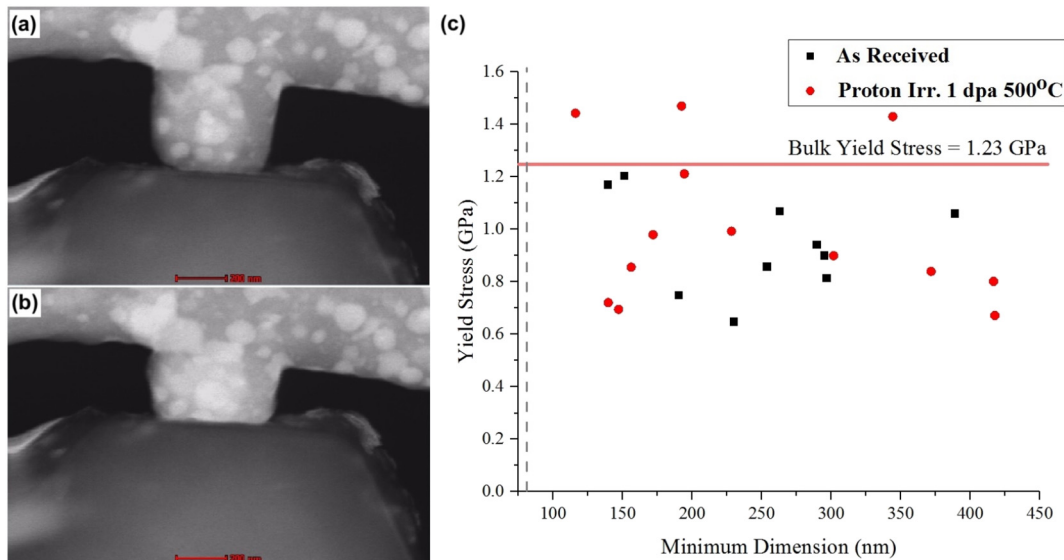

Fig. 3. Representative TEM *in situ* pillar compression still frames from 3 dpa, 500 °C, proton irradiated Cu-10Ta, showing (a) undeformed Cu and Ta phases before compression testing, and (b) dense dislocation network after compression; (c) yield strength as a function of pillar dimension.

and obstacle spacing. Combining the SEM *in situ* pillar results for CRSS from Frick et al. [33] and Dimiduk et al. [34], the transition dimension can be estimated ~4700 nm. Their studies also estimate a defect density based on pure annealed metals, from which one can approximate an average obstacle spacing of ~1000 nm. For this pure Ni data set, an average obstacle spacing is again used to estimate L_{ob} since the microstructural details are known as a volumetric average.

LiF – Soler et al. [35] carry out SEM *in situ* pillar compression tests using a variety of pillar dimensions on LiF. Although their study focused on the role of temperature on CRSS, they obtain a sufficient number of data points using room temperature pillar compression tests, in order to estimate a transition dimension ~1000 nm. They also report a dislocation density, from which an obstacle spacing of ~200 nm can be approximated.

Pure Fe Single Crystals – Rogne & Thaulow [36] conduct compression testing of pure Fe single crystal micropillars loaded along the ⟨001⟩ direction. Pillar diameters range 140 nm to 4.3 μm. They measure 0.2% offset strain yield stress as a function of the pillar diameters, but do not observe a transition dimension. However, when their results are considered in the context of yield stress measurements from thin Fe plates loaded in the [110] direction [37], and tension and compression experiments on single crystal Fe [38–40], a transition dimension of ~10,000 nm can be estimated (see Fig. 7 in ref. [36]). Rogne & Thaulow report an average (*i.e.* not specific to a slip system) dislocation density of 10^{12} m^{-2}, from which an average obstacle spacing of ~1000 nm can be estimated.

Single Crystal Cu (Cantilevers) – Size effect transition dimensions are also identified using cantilever geometries. For example, Motz et al. [41] conduct bending tests on single-crystal Cu micro-cantilevers with beam thicknesses ranging from 7.5 to 1 μm. Flow stress is measured from the plateau load force and plotted against the beam thickness, which reveals a transition dimension ~3 μm (see Fig. 6 in ref. [41]). They suggest a characteristic length of 4 μm for pure Cu based on strain gradient plasticity models.

Ni Films (Flexure) – A load-unload flexure testing geometry is utilized by Ehrler et al. [42] on Ni thin films of thicknesses 10, 50, and 125 μm. The reported grain size of each film thickness is 30 μm; with no other reported microstructural information, this value is used as the approximate obstacle density. Yield stress is reported as a function of the inverse square root of the grain size (see Fig. 3 of ref. [42]), and a transition is evident between films with thickness 10 μm and films with thickness 50 μm. Hence, a transition dimension of 50 μm is used for the discussion herein.

Compiling the transition dimensions and L_{ob} values from all aforementioned studies, a roughly linear relationship can be found between extrinsic and intrinsic size effects, but additional data points should be obtained before a conclusive relationship can be drawn (Fig. 4). The

authors' own results (refs. [13, 14]) fall into agreement with the overall trend. Regions in which intrinsic or extrinsic size effects dominate the mechanical response can be approximated. That is, in Fig. 4, the extrinsic size effect is dominant in the upper left region relative to the data points; here, specimen dimensions are sufficiently larger than microstructural constraints, enabling meaningful yield strengths to be measured. However, the intrinsic size effect is dominant in the lower right region of Fig. 4; here, specimen dimensions are too small relative to the microstructure, so yield strength measurements will be inflated. These regions are shaded only for illustrative purposes and do not abut the data points in order to account for experimental uncertainty and the limited amount of data presented here.

This extrinsic-intrinsic relationship suggests that perfect crystals (*i.e.* infinitely large obstacle spacing) require infinitely large specimen dimensions because of the absence of a dislocation source; this is consistent with the original definition of the size effect, in which defect-free specimens will evaluate near the theoretical strength. At the same time, specimens that possess a high defect density, such as nanostructured and irradiated materials, can be tested at progressively smaller volumes and still provide meaningful quantitative assessment of yield strength. Malyar and coworkers [43] recently showed that micropillar yield strengths will fall along a strength distribution function, and that at least 300–500 specimens must be tested under identical conditions in order to discriminate the nature of this continuous probability distribution. Using the intrinsic-extrinsic relationship herein to inform the specimen geometry could tighten these statistical distributions. Finally, at the intrinsic obstacle spacings found in nanostructured and irradiated materials, the allowable extrinsic pillar dimensions are electron transparent, enabling one to utilize TEM *in situ* pillar compression testing to simultaneously measure mechanical properties and observe plastic phenomena at the nanoscale, representing the potential for unparalleled advancement in our understanding of deformation processes in nanostructured and irradiated materials.

Acknowledgements

Fig. 4. Relationship between extrinsic and intrinsic size effect for compression pillars.

References

[1] E. Arzt, Acta Mater. 46 (1998) 5611–5626.
[2] W.D. Nix, H.J. Gao, J. Mech. Phys. Solids 46 (1998) 411–425.
[3] A.A. Elmustafa, D.S. Stone, Acta Mater. 50 (2002) 3641–3650.
[4] D. Kiener, W. Grosinger, G. Dehm, R. Pippan, Acta Mater. 56 (2008) 580–592.
[5] J.D. Nowak, A.R. Beaber, O. Ugurlu, S.L. Girshick, W.W. Gerberich, Scr. Mater. 62 (2010) 819–822.
[6] J.R. Greer, J.T.M. De Hosson, Prog. Mater. Sci. 56 (2011) 654–724.
[7] A.H.W. Ngan, X.X. Chen, P.S.S. Leung, R. Gu, K.F. Gan, MRS Commun. 7 (2017) 131–140.
[8] T.A. Parthasarathy, S.I. Rao, D.M. Dimiduk, M.D. Uchic, D.R. Trinkle, Scr. Mater. 56 (2007) 313–316.
[9] D. Kiener, P. Hosemann, S.A. Maloy, A.M. Minor, Nat. Mater. 10 (2011) 608–613.
[10] P. Hosemann, Scr. Mater. 143 (2018) 161–168.
[11] G.S. Was, Fundamentals of Radiation Materials Science, Springer, New York, 2007.
[12] B. Girault, A.S. Schneider, C.P. Frick, E. Arzt, Adv. Eng. Mater. 12 (2010) 385–388.
[13] K.H. Yano, M.J. Swenson, Y. Wu, J.P. Wharry, J. Nucl. Mater. 483 (2017).
[14] P.V. Patki, Microstructure Evolution and TEM In Situ Mechanical Testing of Proton Irradiated Nanocrystalline Copper Tantalum Alloy (M.S. Thesis), Purdue University, 2018.
[15] A. Kimura, H.-S. Cho, N. Toda, R. Kasada, K. Yutani, H. Kishimoto, N. Iwata, S. Ukai, M. Fujiwara, J. Nucl. Sci. Technol. 44 (2007) 323–328.
[16] A. De Bremaecker, J. Nucl. Mater. 428 (2012) 13–30.
[17] P. Dubuisson, Y. de Carlan, V. Garat, M. Blat, J. Nucl. Mater. 428 (2012) 6–12.
[18] J. Hoffmann, M. Rieth, R. Lindau, M. Klimenkov, A. Möslang, R.H. Zschommler Sandim, J. Nucl. Mater. 442 (2013) 444–448.
[19] G.R. Odette, JOM 66 (2014) 2427–2441.
[20] S.J. Zinkle, J.L. Boutard, D.T. Hoelzer, A. Kimura, R. Lindau, G.R. Odette, M. Rieth, L. Tan, H. Tanigawa, Nucl. Fusion 57 (2017), 092005.
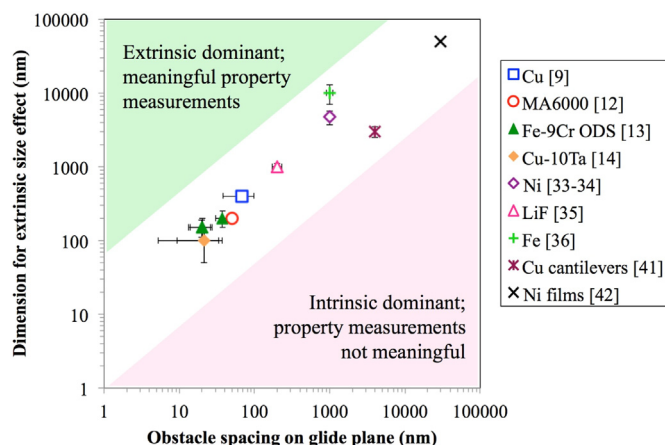
[21] K.A. Darling, M. Rajagopalan, M. Komarasamy, M.A. Bhatia, B.C. Hornbuckle, R.S. Mishra, K.N. Solanki, Nature 537 (2016) 378–381.

[22] L. Toualbi, C. Cayron, P. Olier, R. Logé, Y. de Carlan, J. Nucl. Mater. 442 (2013) 410–416.

[23] C.K. Dolph, D.J. da Silva, M.J. Swenson, J.P. Wharry, J. Nucl. Mater. 481 (2016).

[24] M.J. Swenson, C.K. Dolph, J.P. Wharry, J. Nucl. Mater. 479 (2016) 426–435.

[25] M.J. Swenson, J.P. Wharry, J. Nucl. Mater. 467 (2015) 97–112.

[26] M.J. Swenson, J.P. Wharry, J. Nucl. Mater. 496 (2017) 24–40.

[27] K.H. Yano, S. Thomas, M.J. Swenson, Y. Lu, J.P. Wharry, J. Nucl. Mater. 502 (2018) 201–212.

[28] M.J. Swenson, J.P. Wharry, J. Nucl. Mater. 502 (2018) 30–41.

[29] C.M. Parish, K.G. Field, A.G. Certain, J.P. Wharry, J. Mater. Res. 30 (2015) 1275–1289.

[30] K.A. Darling, M.A. Tschopp, R.K. Guduru, W.H. Yin, Q. Wei, L.J. Kecskes, Acta Mater. 76 (2014) 168–185.

[31] J.R. Greer, J.-Y. Kim, M.J. Burek, JOM 61 (2009) 19–25.

[32] G. Dehm, B.N. Jaya, R. Raghavan, C. Kirchlechner, Acta Mater. 142 (2018) 248–282.

[33] C.P. Frick, B.G. Clark, S. Orso, A.S. Schneider, E. Arzt, Mater. Sci. Eng. A 489 (2008) 319–329.

[34] D.M. Dimiduk, M.D. Uchic, T.A. Parthasarathy, Acta Mater. 53 (2005) 4065–4077.

[35] R. Soler, J.M. Wheeler, H.J. Chang, J. Segurado, J. Michler, J. Llorca, J.M. Molina-Aldareguia, Acta Mater. 81 (2014) 50–57.

[36] B.R.S. Rogne, C. Thaulow, Philos. Mag. 95 (2015) 1814–1828.

[37] M. Fukamachi, Jpn. J. Appl. Phys. 11 (1972) 1259–1264.

[38] W.A. Spitzig, A.S. Keh, Metall. Trans. A. 1 (1970) 2751.

[39] D. Stein, J. Low, Acta Metall. 14 (1966) 1183–1194.

[40] T.L. Altshuler, J.W. Christian, Philos. Trans. R. Soc. A Math. Phys. Eng. Sci. 261 (1967) 253–287.

[41] C. Motz, T. Schöberl, R. Pippan, Acta Mater. 53 (2005) 4269–4279.

[42] B. Ehrler, X.D. Hou, T.T. Zhu, K.M.Y. P'Ng, C.J. Walker, A.J. Bushby, D.J. Dunstan, Philos. Mag. 88 (2008) 3043–3050.

[43] N.V. Malyar, B. Grabowski, G. Dehm, C. Kirchlechner, Acta Mater. 161 (2018) 412–419.